Total and partial photoneutron cross sections for Pb isotopes

T. Kondo,[1] H. Utsunomiya,[1] S. Goriely,[2] I. Daoutidis,[2] C. Iwamoto,[1] H. Akimune,[1] A. Okamoto,[1] T. Yamagata,[1] M. Kamata,[1] O. Itoh,[1] H. Toyokawa,[3] Y.-W. Lui,[4] H. Harada,[5] F. Kitatani,[5] S. Hilaire,[6] and A. J. Koning[7]

[1]*Department of Physics, Konan University, Okamoto 8-9-1, Higashinada, Kobe 658-8501, Japan*

[2]*Institut d'Astronomie et d'Astrophysique, Université Libre de Bruxelles, Campus de la Plaine, CP-226, 1050 Brussels, Belgium*

[3]*National Institute of Advanced Industrial Science and Technology, Tsukuba 305-8568, Japan*

[4]*Cyclotron Institute, Texas A&M University, College Station, Texas 77843, USA*

[5]*Japan Atomic Energy Agency, Tokai-mura, Naka, Ibaraki 319-1195, Japan*

[6]*CEA, DAM, DIF, F-91297 Arpajon, France*

[7]*Nuclear Research and Consultancy Group, P.O. Box 25, NL-1755 ZG Petten, The Netherlands*

(Received 12 June 2012; published 17 July 2012)

Using quasimonochromatic laser-Compton scattering γ rays, total photoneutron cross sections were measured for ^{206,207,208}Pb near neutron threshold with a high-efficiency 4π neutron detector. Partial $E1$ and $M1$ photoneutron cross sections along with total cross sections were determined for ^{207,208}Pb at four energies near threshold by measuring anisotropies in photoneutron emission with linearly polarized γ rays. The $E1$ strength dominates over the $M1$ strength in the neutron channel where $E1$ photoneutron cross sections show extra strength of the pygmy dipole resonance in ^{207,208}Pb near the neutron threshold corresponding to 0.32%–0.42% of the Thomas-Reiche-Kuhn sum rule. Several μ_N^2 units of $B(M1)\uparrow$ strength were observed in ^{207,208}Pb just above neutron threshold, which correspond to an $M1$ cross section less than 10% of the total photoneutron cross section.

DOI: 10.1103/PhysRevC.86.014316 PACS number(s): 25.20.Lj, 24.30.Gd, 27.80.+w

I. INTRODUCTION

There is growing interest to investigate pygmy dipole resonance (PDR) and $M1$ resonance that are built on top of the low-energy tail of the giant dipole resonance (GDR) near the neutron threshold. The PDR and $M1$ resonance constitute extra components of a nuclear statistical quantity, the γ-ray strength function [1], and enhance radiative neutron capture cross sections. Thus, these resonances play a unique role in the γ-ray strength function method [2–4] which is an indirect experimental method of determining radiative neutron capture cross sections for unstable nuclei.

^{208}Pb is a well-studied nucleus for which both $E1$ and $M1$ strengths were investigated in the neutron as well as γ channels. Below the neutron threshold, the nuclear resonance fluorescence (NRF) experiments were carried out to study $E1$ strength with unpolarized bremsstrahlung [5–8], while off-axis polarized bremsstrahlung [9] and highly polarized laser Compton scattering γ-ray beams [10,11] were used in NRF experiments with a focus on $M1$ strength. Above the neutron threshold, the threshold photoneutron technique with bremsstrahlung identified several $M1$ states [12], while measurements of neutron transmission, capture γ ray, and elastic scattering with high-resolution pulsed-neutron beams revealed a large number of $M1$ states [13]. Thus, intensive efforts were made to determine $E1$ and $M1$ strengths for resolved peaks below and above the neutron threshold. In contrast, the determination of full $E1$ and $M1$ strengths including the continuum may not be trivial at all. Very recently, a high-resolution inelastic proton scattering experiment was performed to investigate an electric dipole response of ^{208}Pb by measuring the angular distribution and polarization transfer observables [14,15].

We carried out total photoneutron cross-section measurements for ^{206,207,208}Pb with a high-efficiency 4π neutron detector using quasimonochromatic γ-ray beams. We also performed measurements of total and partial ($E1$ and $M1$) photoneutron cross sections for ^{207,208}Pb just above neutron threshold with an anisotropy neutron detector using linearly polarized γ-ray beams. We discuss total, $E1$, and $M1$ photoneutron cross sections for the lead isotopes.

Details of the experiment are given in Sec. II. The experimental total and partial photoneutron cross sections are compared with model calculations in Sec. III. The present $E1$ and $M1$ strengths in the neutron channel are compared with results of other experiments in Sec. IV. Finally, conclusions are given in Sec. V.

II. EXPERIMENTAL PROCEDURE

A. Total photoneutron cross-section measurements with a 4π detector

Enriched metallic samples of ^{206}Pb (99.30%, 1.56×10^3 mg/cm^2), ^{207}Pb (99.10%, 1.98×10^3 mg/cm^2), and ^{208}Pb (99.70%, 1.99×10^3 mg/cm^2) were irradiated with quasimonochromatic laser-Compton scattering (LCS) γ rays produced at the National Institute of Advanced Industrial Science and Technology. A pencil-like beam of the LCS γ rays were produced in *head-on* collisions between high-intensity Nd:YVO_4 laser photons and relativistic electrons circulating in the Tsukuba Electron Ring for Acceleration and Storage (TERAS) storage ring. The laser was operated in the Q-switch mode at 20 kHz to generate 1064 nm photons at 40 W and 532 nm photons at 24 W with a frequency-doubler module. The electron-beam energy was tuned from 554.1 to 763.0 MeV and the beam current varied from 195 (maximum) to 36 mA (minimum) during the present experiment. The LCS γ-ray beam was produced at 14 energies from 7.0 to 13.5 MeV. The

Compton backscattering γ rays were collimated into 2 mm in diameter with a 20-cm-thick lead collimator. The diameter of the samples was 8.00 mm and the length was 1.39–1.77 mm.

A high-efficiency 4π neutron detector composed of triple rings of 20 ^{3}He proportional counters altogether embedded in a polyethylene moderator was used for neutron detection. The average neutron energy was determined with the ring-ratio technique originally developed by the Livermore group [16], which was applied to the present triple-ring neutron detectors. The detection efficiency was 74%–60% in the energy range less than 1 MeV. Measurements below neutron threshold were carried out for ^{208}Pb at 7.27 MeV and ^{206}Pb at 7.75 MeV. No significant neutron events were observed.

The number of the LCS γ rays incident on the targets was determined from pileup- and single-photon spectra measured with an 8-in.-diameter $\times$12 -in.–length NaI(Tl) detector [17]. The LCS γ-ray beam was measured with a 120% high-purity germanium detector (HPGe) at a reduced laser power. The original energy distribution of the LCS γ ray was determined by a Monte Carlo simulation with the EGS4 code [18] so as to best reproduce the response (energy spectrum) of the HPGe to the LCS γ rays. The measurement was made before and after the photoneutron measurements with the full laser power to monitor time variation of the energy spread. The energy spread of the beam was 4.6%–16.8% in the full width at half maximum (FWHM). The time variation stayed at a few percent in FWHM during 61-84-min. runs immediately above neutron threshold and was otherwise negligible. Note that the LCS γ rays in the energy interval between the neutron threshold and the maximum beam energy are responsible for inducing photoneutron emissions. The energy interval is smaller than the energy spread of the beam in the long runs near neutron threshold. Details of the total photoneutron cross-section measurements are found in Refs. [19,20].

Total photoneutron cross sections were deduced at the average γ-ray energies with the Taylor expansion method [19]. The systematic uncertainty for the cross section is $\pm$4.4% which represents a quadratic sum of uncertainties of the neutron detection efficiency (3.2%) and the number of incident γ rays (3%).

B. Total and partial photoneutron cross-section measurements with an anisotropy detector

Metallic targets of 98.5% 9587 mg ^{208}Pb and a 99.1% 3482 mg ^{207}Pb were irradiated with LCS γ rays. The ^{208}Pb target consisted of a 99.7% 1000 mg sample and a 98.4% 8587 mg sample. The diameter of the two samples enclosed in aluminum containers was 8.00 mm. Linearly polarized LCS γ-ray beams were produced at 7.75, 8.15, 8.60, and 9.05 MeV in the measurement for ^{208}Pb and at 7.35, 7.70, 8.20, and 8.70 MeV for ^{207}Pb, respectively. The degree of polarization of a laser beam was measured with a polarization beam splitter at three positions along the optics system, immediately after the Nd:YVO_4 laser, after a $\lambda/2$ plate, and at an equivalent position as the collision point between laser photons and electrons after passing through such optical elements as an expander, two mirrors, and one lens. The linear polarization was determined to be 93.4 ± 0.7%. The depolarization by inverse Compton scattering into a finite solid angle subtended by the collimator was calculated to be 0.13%–1.2%.

Partial photoneutron cross sections were determined for ^{208}Pb and ^{207}Pb by measuring the anisotropy in photoneutron emission. s-wave ($\ell = 0$) neutrons are emitted after $E1$ photoexcitation of ^{208}Pb and ^{207}Pb, while p-wave neutrons are emitted after $M1$ photoexcitation. Obviously, s-wave neutrons are emitted isotropically.

Defining the linear polarization by the direction of the electric component of the electromagnetic wave (x axis), the angular distribution for p-wave photoneutrons is expressed by

$$W_{\rm pol}(\theta, \phi) = \frac{3}{8\pi}[\sin^2\theta(1 + \cos 2\phi)], \quad (1)$$

where θ stands for the polar angle for photoneutron emission with respect to the beam direction (z axis), while ϕ stands for the azimuthal angle with respect to the x axis.

In the case of unpolarized γ-ray beam with the electric component randomly distributed in the x-y plane, the angular distribution is given by

$$W_{\rm unpol}(\theta, \phi) = \frac{3}{8\pi}\sin^2\theta. \quad (2)$$

Neutron detectors were high- and flat-efficiency long counters of East and Walton [21] with the same detector components, five ^{3}He proportional counters, polyethylene moderator, and twelve neutron-guiding holes. The outer shield was made of borated polyethylene and cadmium sheet of octagonal shape. The experimental setup is depicted in Fig. 1. Four sets of neutron detectors were placed at $\theta = \pi/2$ at the distance of 125 mm between the front face of the detectors and the target; two detectors in the vertical plane at the positions of $\phi = 0$ and π and two in the horizontal plane at the positions of $\phi = \pi/2$ and $3\pi/2$, where the angles are quoted for the vertically polarized beam. The detection efficiency was measured with a calibrated ^{252}Cf source. The result agrees with the Monte Carlo simulation with the MCNP code [22] within 6%.

The four detectors were attached to aluminum frames that are rotatable as a whole detector system along the beam axis. The partial–cross-section measurement was made by rotating the whole detector system by 0° and 90° clockwise by looking downstream of the beamline at each energy. The polarization of the vertically polarized beam was also flipped by 90° with the $\lambda/2$ optical plate. The efficiencies of the four detectors were checked with a ^{241}Am/Be source at the two rotational angles, altogether six times in the course of the experiment. The variation of the efficiency by rotation was 1.6% in the root mean square. The detection efficiencies for s-wave and p-wave photoneutrons induced by the vertically polarized and unpolarized beams were simulated with the MCNP code. Results are shown in Fig. 2.

C. Data reduction

Neglecting higher-order multipoles other than $E1$ and $M1$ in the photoexcitation of ^{208}Pb and ^{207}Pb, the total neutron yield of the two detectors placed parallel to the polarization of

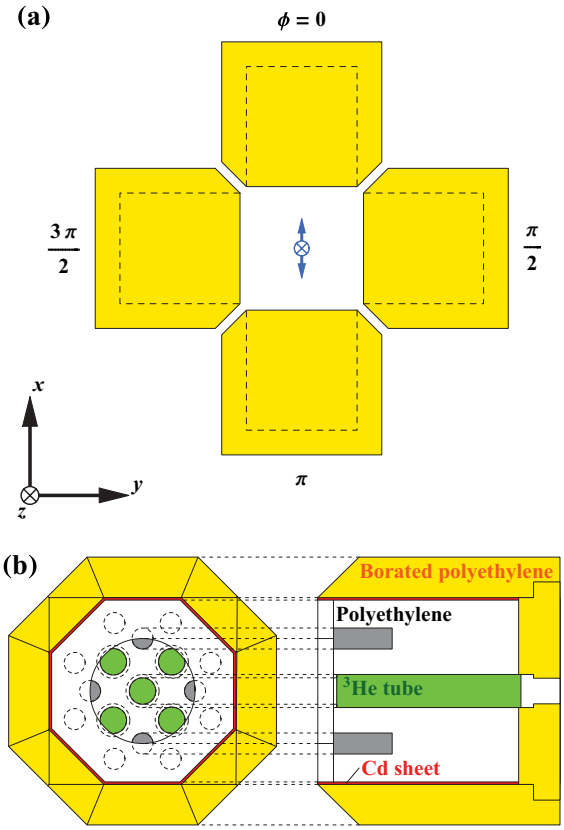

FIG. 1. (Color online) (a) Experimental setup of four sets of neutron detectors for a vertically polarized γ-ray beam. (b) Front and side cross-sectional views of a set of neutron detector.

the beam ($Y_\parallel$) is written as

$$Y_\parallel = 2N_{\rm tot}\{R^0\varepsilon^0 + R^1[P\varepsilon^1_\parallel + (1-P)\varepsilon^1]\}, \tag{3}$$

where $N_{\rm tot}$ is the total number of neutrons emitted in the photodisintegration of current interest, R^0 and R^1 are the probabilities of emitting s-wave and p-wave neutrons, respectively, P is the polarization of the beam, and ε^0, $\varepsilon^1_\parallel$, and ε^1 are, respectively, the detection efficiencies for s-wave neutrons and p-wave neutrons induced by the polarized and unpolarized beams. Note that the four detectors have the same efficiencies for s-wave neutrons and p-wave neutrons, respectively, induced by unpolarized beam.

Similarly, the total neutron yield of the two detectors placed perpendicular to the polarization of the beam ($Y_\perp$) is written with the corresponding quantities as

$$Y_\perp = 2N_{\rm tot}\{R^0\varepsilon^0 + R^1[P\varepsilon^1_\perp + (1-P)\varepsilon^1]\}. \tag{4}$$

Note that $\varepsilon^1_\parallel + \varepsilon^1_\perp = 2\,\varepsilon^1$. In Eqs. (3) and (4), $Y_\parallel$, $Y_\perp$, P, ε^0, $\varepsilon^1_\parallel$, $\varepsilon^1_\perp$, and ε^1 are experimentally known quantities. The detection efficiencies are given in Fig. 2. Under the present assumption,

$$R^0 + R^1 = 1, \tag{5}$$

so that only the two quantities (for example $N_{\rm tot}$ and R^1) are unknown.

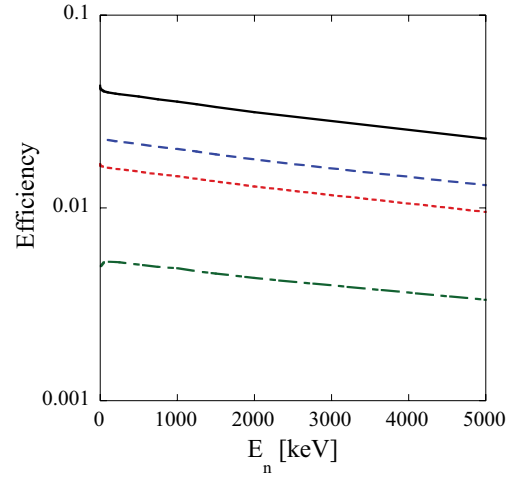

FIG. 2. (Color online) Detection efficiencies of neutron detector for p-wave neutrons induced by a polarized γ-ray beam for detector placed along polarization (solid line, $\varepsilon^1_\parallel$) and perpendicular to the polarization (dot-dashed line, $\varepsilon^1_\perp$) and for p-wave neutrons induced by unpolarized γ-ray beam (dashed line, ε^1); and for s-wave neutrons (dotted line, ε^0).

Introducing the quantity Σ,

$$\Sigma = \frac{1}{P}\frac{Y_\parallel - Y_\perp}{Y_\parallel + Y_\perp}, \tag{6}$$

one can solve Eqs. (3) and (4) to obtain

$$R^0 = \frac{A - \Sigma}{A - \Sigma(1 - \varepsilon^0/\varepsilon^1)}, \tag{7}$$

$$R^1 = \frac{\varepsilon^0\Sigma/\varepsilon^1}{A - \Sigma(1 - \varepsilon^0/\varepsilon^1)}, \tag{8}$$

and

$$N_{\rm tot} = \frac{Y_\parallel + Y_\perp}{4(\varepsilon^0 R^0 + \varepsilon^1 R^1)}. \tag{9}$$

Here A is the analyzing power of our detector system:

$$A = \frac{\varepsilon^1_\parallel - \varepsilon^1_\perp}{2\varepsilon^1}. \tag{10}$$

The total cross section $\sigma_{\rm tot}$ and the partial cross sections σ_{E1} and σ_{M1} are given with the number of incident γ rays, N_γ, and the areal density of the target nuclei N_t as follows:

$$\sigma_{\rm tot} = \frac{N_{\rm tot}}{N_t N_\gamma}, \tag{11}$$

$$\sigma_{E1} = R^0\sigma_{\rm tot}, \tag{12}$$

$$\sigma_{M1} = R^1\sigma_{\rm tot}. \tag{13}$$

The statistical and systematic uncertainties of the cross sections were estimated from an error propagation of those, respectively, associated with the neutron yields ($Y_\parallel$ and $Y_\perp$) and the polarization (P), the neutron detection efficiencies (ε), and the number of γ rays (N_γ). The resultant $E1$ and $M1$ cross sections for ^{208}Pb and ^{207}Pb are given in Tables I and II, respectively.

TABLE I. $E1$ and $M1$ photoneutron cross sections for ^{208}Pb along with statistical and systematic uncertainties.

E (MeV)	$\sigma(E1)$ (mb)	$\Delta\sigma_{stat}$ (mb)	$\Delta\sigma_{syst}$ (mb)	$\sigma(M1)$ (mb)	$\Delta\sigma_{stat}$ (mb)	$\Delta\sigma_{syst}$ (mb)
7.51	39.31	2.56	2.59	0.66	1.29	0.08
7.77	28.52	1.38	1.82	1.90	0.73	0.22
8.16	28.20	1.28	1.79	3.09	0.69	0.36
8.32	33.19	0.82	2.13	1.86	0.42	0.21

III. COMPARISON WITH THEORY

The newly measured cross sections are now compared with theoretical estimates. The photoneutron emission is determined with the TALYS reaction code [23] and different γ-ray strength functions; namely, the Lorentzian and generalized Lorentzian models [1], as well as more microscopic models based on the mean-field approach plus the random phase approximation (RPA). ^{208}Pb has been widely studied within the relativistic and nonrelativistic mean-field plus RPA models using many different interactions and is a nucleus free from uncertainties related to deformation effects and pairing correlation (see, for example, Refs. [24,25]). Qualitatively, most of the RPA calculations predict a GDR centroid energy close to experimental photoabsorption data. They also find some extra low-lying strength in the vicinity of the neutron threshold (i.e., around 7.4 MeV), as confirmed by our new experimental data and by previous high-resolution (γ,γ') [6] or (p,p') [14] experiments. However, quantitatively, significant differences are found for different interactions in the specific determination of the pygmy resonance (PR) energy and strength.

In Fig. 3, experimental data, including our newly measured cross sections, are compared with the predictions based on the Lorentzian and generalized Lorentzian models [1] as well as the nonrelativistic Hartree-Fock-Bogoliubov and quasiparticle random phase approximation (HFB + QRPA) systematics [26]. Note that, following Ref. [27], Saclay data [28] need to be renormalized down by 7% and Livermore data [29] up by 22%. While the Lorentzian approximation clearly overestimate the cross section at low energies, the generalized Lorentzian underestimate it. The nonrelativistic HFB + QRPA gives a fair description but fails to describe the threshold behavior (i.e., the extra strength found at the neutron threshold). The present HFB + QRPA calculation is based on the BSk7 Skyrme force, while other interactions with larger-symmetry energy or L coefficients (where L is the

TABLE II. $E1$ and $M1$ photoneutron cross sections for ^{207}Pb along with statistical and systematic uncertainties.

E (MeV)	$\sigma(E1)$ (mb)	$\Delta\sigma_{stat}$ (mb)	$\Delta\sigma_{syst}$ (mb)	$\sigma(M1)$ (mb)	$\Delta\sigma_{stat}$ (mb)	$\Delta\sigma_{syst}$ (mb)
7.02	16.03	1.63	1.04	2.97	0.98	0.35
7.24	24.53	2.22	1.56	2.99	1.24	0.34
7.52	25.80	1.69	1.63	2.65	0.91	0.30
8.11	31.03	6.56	2.16	−0.94	3.03	0.11

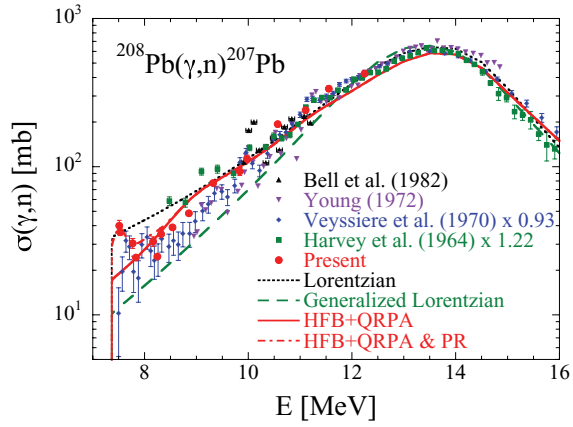

FIG. 3. (Color online) Comparison between experimental and theoretical ^{208}Pb$(\gamma,n)^{207}$Pb cross sections. Predictions are obtained with the Lorentzian and generalized Lorentzian models [1] as well as HFB + QRPA $E1$ strengths [26]. Experimental data are taken from Refs. [28–31] in addition to the present data.

density derivative of the symmetry energy at saturation) could potentially lead to a stronger PR [25].

Similar comparisons are shown in Fig. 4 where relativistic mean field plus RPA calculations (RRPA) are shown for different meson exchange [24] or point-coupling interactions [32,34]. For the latter case of the continuum RPA, excitations to the continuum are taken into account explicitly. Note that, for all models, the $E1$ strength distribution is renormalized to reproduce the experimental location and width of the GDR [1]. The renormalization procedure is described in Ref. [33]. This can imply an energy shift of a few hundred keVs upward that also shifts the PR close to or above the neutron threshold, especially for the point-coupling interactions. The DDPC1 interaction with a low symmetry energy ($J = 33$ MeV) and L coefficient ($L = 70$ MeV) gives rise to a relatively weak PR strength with respect to the other PCF1, PCLA, and NL3 interactions, but the PR centroid energy is shifted to high

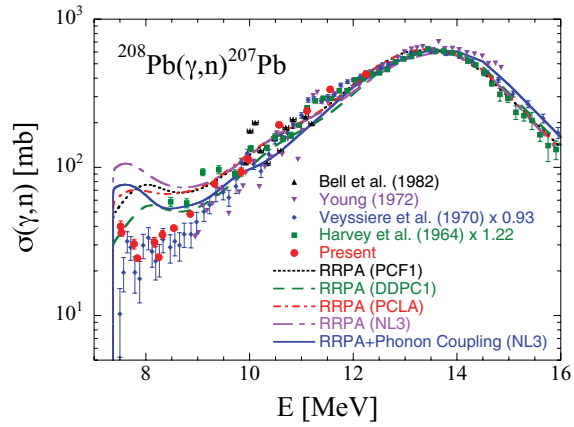

FIG. 4. (Color online) Same as Fig. 3 where the predictions correspond to relativistic mean field (RMF) plus RPA calculations with the point-coupling interactions (PCF1, PCLA, and DDPC1) [32,33] as well as the NL3 interaction with or without taking into account particle-vibration coupling [24].

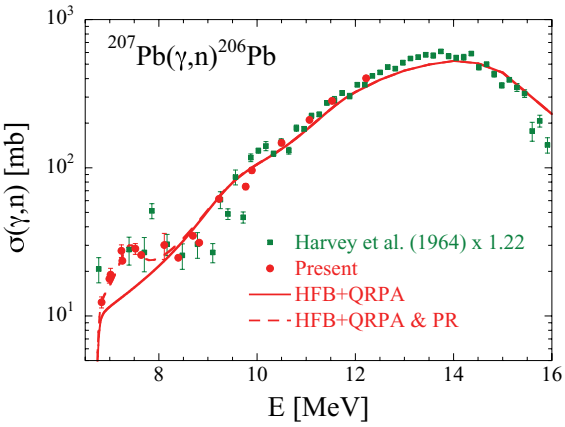

FIG. 5. (Color online) Same as Fig. 3 for ^{207}Pb(γ,n)^{206}Pb.

values, around 8 MeV, some 500 keVs above the neutron threshold, in disagreement with experimental data. In the case of the NL3 interaction ($J = 37.4$ MeV and $L = 118$ MeV), the inclusion of the phonon coupling [24] improves the agreement, but the $E1$ strength still overestimates the (γ,n) data. Similar conclusions on the overestimate of RRPA models were drawn from the analysis of the polarized proton inelastic scattering [14]. The inclusion of the phonon coupling on an interaction like DDPC1 would probably provide a γ-ray strength closer to the data.

As shown in Figs. 3–5, our (γ,n) data confirm the existence of a low-energy PR in the vicinity of the neutron threshold observed in Refs. [6,14]. To highlight its presence, the HFB + QRPA strength supplemented by a pygmy dipole strength is shown to be in good agreement with our low-energy data. The PR is parametrized by a centroid energy of 7.5 MeV, a width of 0.4 MeV, and a cross section at peak energy of about 20 mb for ^{208}Pb and 15 mb for ^{207}Pb in Lorentzian shape. This dipole PR is also confirmed by the partial $E1$ cross section σ_{E1} separately determined as described in the previous section. We compare in Fig. 6 the partial $E1$ cross section with the HFB + QRPA estimate supplemented with the above-mentioned PR for ^{208}Pb (upper panel) and ^{207}Pb (lower panel). The $E1$ PR dominates the total strength in this region though the strength in the unit of the Thomas-Reiche-Kuhn (TRK) sum rule remains small: 0.42% for ^{208}Pb and 0.32% for ^{207}Pb.

In contrast, the M1 partial cross section can be described (see upper panel of Fig. 7) by a simple Lorentzian shape of peak energy $E = 8.06$ MeV, width $\Gamma = 0.6$ MeV, and peak cross section $\sigma_0 = 3.6$ mb. Although these resonance parameters

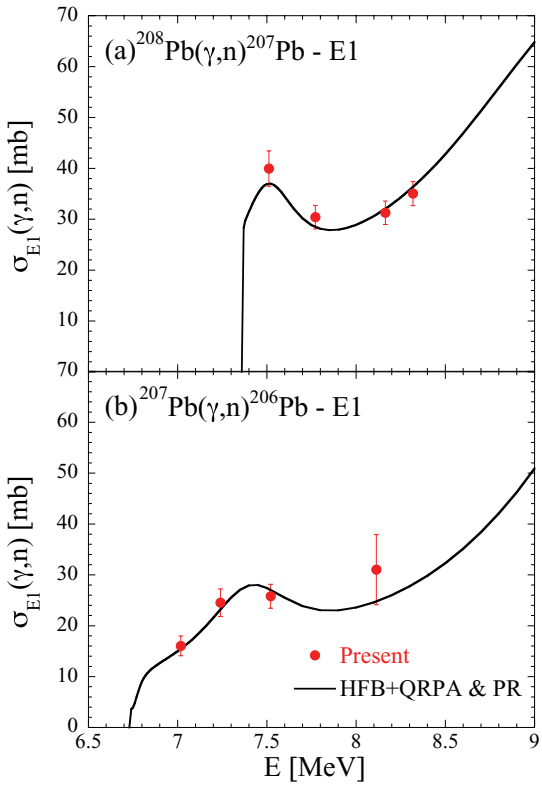

FIG. 6. (Color online) (a) Comparison between experimental and theoretical ^{208}Pb(γ,n)^{207}Pb partial $E1$ cross sections. The solid line corresponds to the HFB + QRPA $E1$ strength [26] with a parametrized PR as described in the text. (b) Same as the upper panel for the ^{207}Pb(γ,n)^{206}Pb partial $E1$ cross section.

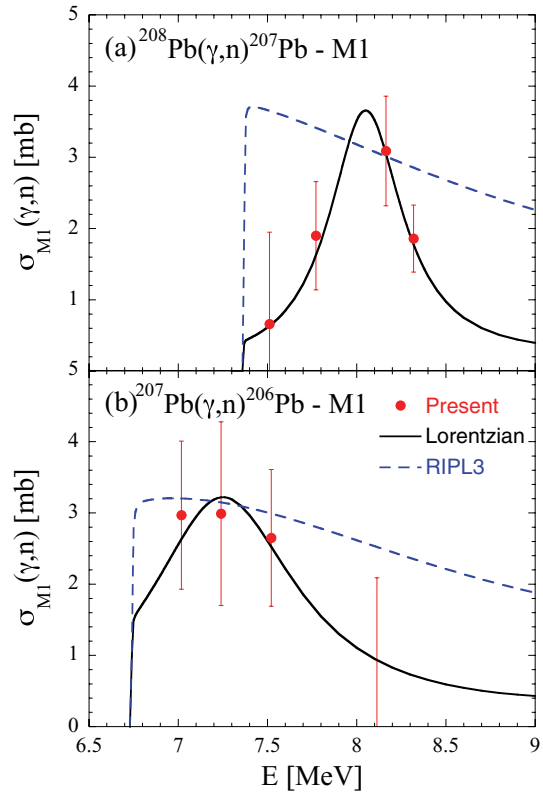

FIG. 7. (Color online) (a) Comparison between experimental and theoretical ^{208}Pb(γ,n)^{207}Pb partial $M1$ cross sections. The solid line corresponds to a simple Lorentzian of peak energy $E = 8.06$ MeV, width $\Gamma = 0.6$ MeV, and peak cross section $\sigma_0 = 3.6$ mb. The dashed line corresponds to the RIPL3 prediction [1] assuming the same peak cross section as in the Lorentzian case. (b) Same as the upper panel for the ^{207}Pb(γ,n)^{206}Pb partial $M1$ cross section and a Lorentzian (solid line) of $E = 7.25$ MeV, $\Gamma = 1$ MeV, and peak cross section $\sigma_0 = 3.2$ mb.

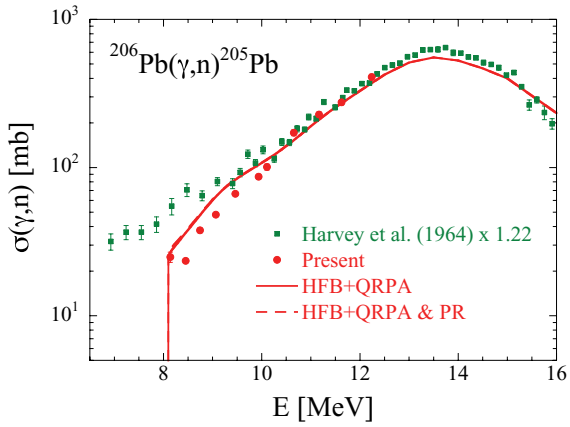

FIG. 8. (Color online) Same as Fig. 3 for ^{206}Pb(γ,n)^{205}Pb.

remain rather uncertain, the M1 strength differs significantly from the usual parametrization proposed by systematics; in particular the RIPL-3 library [1] gives a centroid energy at lower energy (around 6.9 MeV) and a much wider distribution (of width of about 4 MeV). In the ^{207}Pb case, a proper determination of a Lorentzian profile for the $M1$ cross section remains difficult due to the large uncertainties affecting the measurements. The $M1$ cross section is, however, compatible with a Lorentzian shape of peak energy $E \simeq 7.25$ MeV, width $\Gamma \simeq 1$ MeV, and peak cross section $\sigma_0 \simeq 3.2$ mb.

Finally, our new data for ^{206}Pb(γ,n)^{205}Pb are compared with the renormalized Livermore data [29] and the HFB + QRPA estimate with and without the inclusion of a PR of similar strength and centroid energy as the one adopted for ^{208}Pb (Fig. 8). The neutron threshold is, however, in this case relatively higher than the PR energy, so that the (γ,n) data are not sensitive to the presence of a low-lying PR.

IV. $E1$ AND $M1$ STRENGTHS IN ^{208}Pb AND ^{207}Pb IN NEUTRON CHANNEL

The reduced $E1$ transition probability $B(E1)\uparrow$ obtained for ^{208}Pb from the present $E1$ cross sections is 0.82 ± 0.09 e^{2}fm^2 over the $E = 7.51$–8.32 MeV energy range. The high-resolution inelastic proton scattering found a larger $E1$ strength in ^{208}Pb above the neutron threshold, $B(E1)\uparrow = 0.982 \pm 0.206$ e^{2}fm^2 over $E = 7.515$–8.430 MeV [15]. The present $E1$ strength agrees well with that found in the (p, p') measurement.

Similarly, the reduced $M1$ transition probability $B(M1)\uparrow$ obtained for ^{208}Pb from the present $M1$ cross sections is 4.2 ± 2.3 μ_N^2 over $E = 7.51$–8.32 MeV. The neutron-beam measurement [13] found 6.8 μ_N^2 over 7.37–8.67 MeV for resolved peaks with 1^+ assignment. We note that, although the $M1$ strengths of the two measurements reasonably agree with each other, the profile of the strength distribution is quite different; a large concentration of $M1$ strength is seen around 7.5 MeV in the neutron-beam measurement, while the $M1$ strength peaks around 8.1 MeV in the present measurement (Fig. 7).

The present measurement also found for ^{207}Pb, $B(E1)\uparrow = 0.88 \pm 0.17$ e^{2}fm^2 over 7.02–8.32 MeV and $B(M1)\uparrow = 4.0 \pm 1.9$ μ_N^2 over 7.02–7.52 MeV, respectively.

V. CONCLUSION

In addition to total photoneutron cross section measurements for $^{206,\,207,\,208}$Pb with a high-efficiency 4π detector, partial photoneutron cross-section measurements were carried out for $^{207,\,208}$Pb near neutron threshold with polarized laser-Compton scattering γ-ray beams by observing anisotropies in photoneutron emission. The partial cross sections represent full $E1$ and $M1$ strengths consisting not only of resolved peaks but also of the continuum. The $E1$ strength is in good agreement with that determined by the high-resolution inelastic proton scattering [15]. The $E1$ photoneutron cross sections clearly indicate the presence of a pygmy dipole resonance in $^{207,\,208}$Pb near the neutron threshold. The total photoneutron cross sections of lead isotopes are well reproduced with the HFB + QRPA model of the γ-ray strength function supplemented with a pygmy dipole resonance corresponding to 0.32%–0.42% of the TRK sum rule. Several μ_N^2 units of $M1$ strength were found in $^{207,\,208}$Pb near neutron threshold, corresponding to 5.5%–8.2% of the total photoneutron cross sections.

ACKNOWLEDGMENTS

This work is supported by the Japan Private School Promotion Foundation and the JSPS-FNRS bilateral project. S. G. and I. D. acknowledge the financial support of the "Actions de recherche concertées (ARC)" from the "Communauté française de Belgique" and from the FRS-FNRS.

[1] R. Capote *et al.*, Nucl. Data Sheets **110**, 3107 (2009).
[2] H. Utsunomiya *et al.*, Phys. Rev. C **82**, 064610 (2010).
[3] H. Utsunomiya *et al.*, Phys. Rev. C **81**, 035801 (2010).
[4] H. Utsunomiya *et al.*, Phys. Rev. C **84**, 055805 (2011).
[5] T. Chapuran, R. Vodhanel, and M. K. Brussel, Phys. Rev. C **22**, 1420 (1980).
[6] N. Ryezayeva *et al.*, Phys. Rev. Lett. **89**, 272502 (2002).
[7] J. Enders *et al.*, Nucl. Phys. A **724**, 243 (2003).
[8] R. Schwengner *et al.*, Phys. Rev. C **81**, 054315 (2010).
[9] R. M. Laszewski, R. Alarcon, D. S. Dale,and S. D. Hoblit, Phys. Rev. Lett. **61**, 1710 (1988).
[10] H. Ohgaki *et al.*, in *Proceedings of the International Conference on Nuclear Structure and Related Topics*, edited by S. N. Ershov, R. V. Jolos, and V. V. Voronov (Dubna, 1997) (American Institute of Physics, 2009) p. 74.
[11] T. Shizuma *et al.*, Phys. Rev. C **78**, 061303(R) (2008).
[12] C. D. Bowman *et al.*, Phys. Rev. Lett. **25**, 1302 (1970).

[13] R. Köhler, J. A. Wartena, H. Weigmann, L. Mewissen, F. Poortmans, J. P. Theobald, and S. Raman, Phys. Rev. C **35**, 1646 (1987).
[14] A. Tamii *et al*., Phys. Rev. Lett. **107**, 062502 (2011).
[15] I. Poltoratska *et al*., Phys. Rev. C **85**, 041304(R) (2012).
[16] B. L. Berman and S. C. Fultz, Rev. Mod. Phys. **47**, 713 (1975).
[17] T. Kondo *et al*., Nucl. Instrum. Methods A **659**, 462 (2011).
[18] W. R. Nelson, H. Hirayama, and W. O. Rogers, *The EGS4 Code System, SLAC-Report-265* (1985).
[19] H. Utsunomiya *et al*., Phys. Rev. C **80**, 055806 (2009).
[20] A. Makinaga *et al*., Phys. Rev. C **79**, 025801 (2009).
[21] L. V. East and R. B. Walton, Nucl. Instrum. Meth. **72**, 161 (1969).
[22] J. F. Briesmeister, computer code MCNP, Version 5 (Los Alamos National Laboratory, Los Alamos, 2000).
[23] A. J. Koning, S. Hilaire, and M. Duijvestijn, in *Proceedings of the International Conference on Nuclear Data for Science and Technology*, edited by O. Bersillon *et al*. (Nice, 2007) (EDP Sciences, 2008), p. 211.
[24] E. Litvinova, P. Ring, and D. Vretenar, Phys. Lett. B **647**, 111 (2007).
[25] X. Roca-Maza, G. Pozzi, M. Brenna, K. Mizuyama, and G. Colò, Phys. Rev. C **85**, 024601 (2012).
[26] S. Goriely, E. Khan, and M. Samyn, Nucl. Phys. A **739**, 331 (2004).
[27] *Handbook on Photonuclear Data for Applications*, IAEA-TECDOC-1178 (2000).
[28] A. Veyssiere, H. Beil, R. Bergere, P. Carlos, and A. Lepretre, Nucl. Phys. A **159**, 561 (1970).
[29] R. R. Harvey, J. T. Caldwell, R. L. Bramblett, and S. C. Fultz, Phys. Rev. **136**, B126 (1964).
[30] Z. W. Bell, L. S. Cardman, and P. Axel, Phys. Rev. C **25**, 791 (1982).
[31] L. M. Young, Ph.D. thesis, University of Illinois, 1972.
[32] I. Daoutidis and P. Ring, Phys. Rev. C **83**, 044303 (2011).
[33] I. Daoutidis and S. Goriely, Phys. Rev. C (to be published).
[34] J. Daoutidis and P. Ring, Phys. Rev. C **80**, 024309 (2009).